Searching for Physics Beyond the Standard Model with a Rare Decay

Luke A. Corwin*

1 Introduction

1.1 Units, Symbols, and Nomenclature

Particle physics studies the fundamental laws and constituents of the Universe. In particle physics, particles are conventionally represented by symbols as in Table 1. Particle reactions and decays are written in a manner similar to that of chemistry and nuclear physics, with symbols on either side of an arrow ($\rightarrow$); the particles on the left side of the arrow are present before the decay or reaction; the particles on the right side are present afterward. For instance, $n \rightarrow pe^{-}\bar{\nu}_e$ represents a neutron decaying into a proton, electron, and anti-neutrino.

Einstein's Special Theory of Relativity relates mass, energy, and momentum through

$$E^2 = (|\vec{p}|c)^2 + (mc^2)^2 \Rightarrow m = \frac{1}{c^2}\sqrt{E^2 - (|\vec{p}|c)^2}. \quad (1)$$

If a particle is at rest ($|\vec{p}| = 0$), Equation 1 reduces to the famous $E = mc^2 \Rightarrow m = \frac{E}{c^2}$. The standard unit of energy in particle physics is the electron volt (eV), which is the energy required to move an electron through an electric potential difference of 1 volt (Halliday *et al.* 1997). In this paper, mass is written in units of MeV/c^2 or GeV/c^2, where $1\ \mathrm{GeV}/c^2 = 1000\ \mathrm{MeV}/c^2 = 10^9\ \mathrm{eV}/c^2$, and momentum in units of MeV/c or GeV/c.

For every particle, an anti-particle exists with equal mass but opposite charge. Anti-particles are denoted with either a bar over the particle symbol (e.g. $\bar{\nu}_e$) or the opposite charge in a superscript (e.g. e^{+}). When a particle and anti-particle collide, they undergo a process called annihilation, in which both disappear and an equal amount of mass and energy appear in their place in accordance with various laws and probabilities of Quantum Mechanics. Unless otherwise stated, when a particle or equation is given, all statements and numbers related to that particle or equation are also applicable when all charges are reversed and all matter and anti-matter are interchanged. For example, if $n \rightarrow pe^{-}\bar{\nu}_e$ were referenced, all statements about it are assumed to be valid for $\bar{n} \rightarrow \bar{p}e^{+}\nu_e$.

Most particles studied have short lifetimes. They can only travel microscopic distances from appearance to decay and so cannot reach active detector elements. Information about these particles must reconstructed from Special Relativity and measurements of those decay products that have long enough lifetimes to reach detector elements.

1.2 The Standard Model

The Standard Model (SM) is the theory of particle physics; it contains six quarks and six leptons, which are the fundamental particles constituting ordinary matter. Three leptons are charged; for each one, a neutral lepton known as a neutrino exists. They are summarized in Table 1. Within the SM, the behavior of matter and energy is governed by three interactions: weak, strong, and electromagnetism. Electromagnetism affects all charged particles and electromagnetic radiation ; in everyday contexts, it determines the chemical properties of atoms by governing the interactions of electrons with protons and each other. The strong

*Department of Physics, 191 West Woodruff Avenue, Columbus, OH 43210, My primary collaborators on this analysis were Dr. Stephen J. Sekula of the Massachusetts Institute of Technology and Dr. Paul D. Jackson at the Italian National Institute of Nuclear Physics (INFN). My adviser is Prof. Klaus Honscheid of the Ohio State Physics Department. I also wish to acknowledge the invaluable support of the entire *BABAR* collaboration.

interaction affects only quarks and particles made of quarks, which are called hadrons; it is effective only over short ranges on the order of nuclear size. It binds quarks together in hadrons and protons and neutrons together in nuclei; therefore, it is critical for determining the behavior of nuclear fission in nuclear reactors and nuclear fusion inside of stars. Leptons are not affected by the strong interaction.

The weak interaction affects all known particles. As its name suggests, its effects are so small that they are only noticeable when the strong and electromagnetic interactions cannot act. It also affects certain kinds of radioactive decay. Neutrinos are neutral and not affected by the strong force. Therefore, any process involving neutrinos on the subatomic scale is sensitive to the weak interaction. Neutrinos react with matter so weakly and rarely that they are undetectable by most particle physics detectors, including *BABAR*, which is the detector used for this analysis (see Section 2).

Quarks are always found bound to other quarks, which makes many of their individual properties, such as mass and lifetime, difficult to determine or even define. A bound state of a quark and an anti-quark is known as a meson. A bound state of three quarks is known as a baryon; familiar examples include the proton and neutron. The properties of several mesons and baryons relevant to this paper are given in Table 2.

During the past thirty years, the SM has become one of the most thoroughly experimentally verified theories in science. However, we know it is not complete because it does not solve certain problems. The SM cannot account for gravity. It does not predict the masses of the fundamental particles; those must be experimentally determined. It does not account for Dark Matter and Dark Energy, which constitute approximately 96% of the Universe.

Many hypotheses have been proposed beyond the SM to solve some or all of these problems. Any such hypothesis must make predictions that are consistent with the vast array of experimental and observational results confirming the SM. Therefore, each new result that confirms the SM places constraints on any hypothesis beyond the SM. Constraining, eliminating, or supporting hypotheses beyond the SM is a necessary step toward achieving a more complete understanding of the most fundamental laws governing physical reality.

1.3 Current Predictions

My analysis focuses on the charged B meson: $B^+ = \bar{b}u$ and $B^- = b\bar{u}$. This meson has approximately five times the mass of the neutron. It is very unstable and can decay into many different sets of final particles. The fraction of decays resulting in a given set is called the branching fraction ($\mathcal{B}$) of that set. The charged B is the lightest meson that contains a b. Conservation of energy forces the daughters of decaying particles to have a total mass less than that of their parent particle. Thus, no daughters of the charged B can contain b quarks, and the decay of the charged B must change the b into another kind of quark; only the weak interaction can accomplish this.

In a decay with only leptons in the final state, no particles experiencing the strong interaction are produced; therefore, the effects of the strong and weak interactions upon the branching fraction could be easily separated and studied. The strong interaction effects are represented by the parameters $|V_{ub}|$, f_B, and G_F. $|V_{ub}|$ quantifies the probability of a b decaying to a set of final particles containing a u (Cabbibo 1963; Kobayashi and Maskawa 1973); f_B quantifies the proximity of the two quarks within the charged B; G_F quantifies the overall strength of the weak interaction. The simplest type of fully leptonic charged B decay is $B^+ \to \ell^+\nu_\ell$ ($\ell = e, \mu, \tau$), shown in Figure 1.

Somewhat counter-intuitively, complex properties of the weak interaction suppress the branching fractions for $B^+ \to \mu^+\nu$ and $B^+ \to e^+\nu$ by factors of $\sim 5 \times 10^{-3}$ and $\sim 10^{-7}$ with respect to $B^+ \to \tau^+\nu_\tau$.

The quantitative SM prediction is given by:

$$\mathcal{B}(B^+ \to \ell^+\nu_\ell) = \frac{G_F^2 m_B m_\ell^2}{8\pi}\left[1 - \frac{m_\ell^2}{m_B^2}\right]^2 \tau_{B^+} f_B^2 |V_{ub}|^2, \tag{2}$$

where τ_{B^+} is the B^+ lifetime, and m_B and m_ℓ are the B^+ meson and ℓ masses. In this equation, we set $c = 1$.

A search for $B^+ \to \tau^+\nu_\tau$ is experimentally challenging because, unlike the μ or e, the τ has a short enough lifetime to decay within the detector, and charged lepton decays always produce at least one undetectable neutrino. This difficulty is less than the challenge presented by the suppression of the other $B^+ \to \ell^+\nu_\ell$ decay channels, so I present in this paper our attempt to measure $\mathcal{B}(B^+ \to \tau^+\nu_\tau)$.

Except for f_B, all of the quantities in Equation 2 have been measured independently of our analysis. Substituting the measured values of those parameters (Particle Data Group 2006) and $f_B = 0.216 \pm 0.022$ GeV from SM theoretical calculations (HPQCD Collaboration 2005), we obtain a branching fraction of $(1.6 \pm 0.4) \times 10^{-4}$. If we were to measure a much larger branching fraction than the SM predicts, that would imply that f_B is significantly different from the SM prediction, which would be strong evidence of physics beyond the SM. In fact, we find a branching fraction of $(0.9 \pm 0.7(\text{stat.}) \pm 0.1(\text{syst.})) \times 10^{-4}$.

2 The *BABAR* Detector and Dataset

Pairs of charged B mesons are produced by the PEP-II collider at the Stanford Linear Accelerator Center via collisions of electrons (e^-) and anti-elections (known as positrons, e^+) at high energies. Collisions are achieved by crossing beams of e^- and e^+ circulating in opposite directions; when they collide, the resulting annihilation has several possible outcomes through the reaction $e^+e^- \to f\bar{f}$ ($f = u, d, s, c, b, e, \mu,$ or τ) . Given sufficient energy ($> 2m_f c^2$), every collision has a significant probability for producing each possible final state. The greatest probability of producing B mesons occurs at the collision energy 10.58 GeV because 10.58 GeV/c^2 is the mass of the $\Upsilon(4S) = b\bar{b}$. When the $\Upsilon(4S)$ is produced, it decays very quickly into either B^+B^- or $B^0\overline{B}^0$.

Normally, PEP-II is operated at the optimum conditions for producing the $\Upsilon(4S)$. The data produced in this way are called "on-resonance." Approximately 6.2% of of the data is collected with a total energy 40 MeV below the energy necessary to generate the $\Upsilon(4S)$. This "off-resonance" data sample is also below the energy necessary to produce charged B mesons, so we know that it will not contain our signal. Therefore, it is a valuable sample for estimating our background.

Each collision is called an "event." Data from these collisions are collected by the *BABAR* detector. *BABAR* has the shape of a large hexagonal prism surrounding the collision point, as shown in Figure 2. Charged particles are detected via tracks of ions they produce in a chamber of gas within *BABAR*. Neutral particles are detected by the energy they deposit in scintillating crystals. Most of *BABAR* is immersed in a 1.5 T uniform magnetic field generated by a large superconducting solenoidal coil. The magnetic field enables the measurement of charged particle momenta because the path of a charged particle in a magnetic field depends on the particle's momentum (*BABAR* Collaboration 2002). The data sample used in this analysis contains 320×10^6 charged B mesons.

Large samples of simulated data, which is called Monte Carlo (MC), are used to develop and refine the analysis technique, calculate errors, and optimize signal selection cuts. Comparing simulated and real data is essential to ensuring and proving that we understand the detector. When simulated and real data disagree, the source of the disagreement must be understood and resolved, or the magnitude of the disagreement is included in our result as a systematic uncertainty. We used the GEANT4 (GEANT4 Collaboration 2003) software package to generate MC for this analysis.

3 Analysis Method

Since the τ has a short lifetime of $(290.6 \pm 1.0) \times 10^{-15}$ seconds, it must be reconstructed from its decay products. We use the four most common decay channels, which are shown in Table 3 and together constitute

approximately 71% of the τ branching fraction. Each channel contains at least one neutrino. To overcome the difficulties presented by undetectable neutrinos, we employ and refine a technique called "tagging" that accounts for all detectable results of the decay.

3.1 Tag B Reconstruction

Since the charged B mesons are always produced in B^+B^- pairs, we reconstruct one of them (the "tag" B) in a well understood and measured set of decay channels ($B^- \to D^0\ell^-\bar{\nu}_\ell X$), where ℓ represents either e or μ. X can be either nothing or an unreconstructed particle from the case where the D^0 is a daughter of a higher mass particle. We use this method because once the tag has been reconstructed, we know that whatever remains in the event should have been produced a real charged B (the "signal" B). We can then examine those products for the signature of $B^+ \to \tau^+\nu_\tau$.

The data sample is reduced in size several times as portions of the sample are cut away. The first set of these cuts is applied by the collaboration to isolate those collision events that are likely to contain at least one $B^- \to D^0\ell^-\bar{\nu}_\ell X$decay. We further refine this sample though further cuts on important kinematic and angular quantities. Cuts are tested and optimized on simulated data to determine which variables and cuts will maximize the signal to background ratio.

$D^0\ell$ candidates are reconstructed by combining a D^0 with an e or μ. The technical details of these cuts include requiring the tag side lepton to have momentum above $0.8\ \mathrm{GeV}/c$ in the center-of-mass (CM) frame, where the colliding electron and positron have equal and opposite momentum. The D^0 and ℓ candidates are required to meet at a common vertex. The flight direction and mass of the daughter and reconstructed particles are also used to cut away unwanted background.

After all cuts have been applied to the tag B, $(0.664 \pm 0.003)\%$ of the original B^+B^- data sample remains. This small efficiency is worthwhile because without the tag, the number of neutrinos in each event would make our signal indistinguishable from a myriad of background decays.

3.2 Selection of $B^+ \to \tau^+\nu_\tau$ Signal

After the tag B reconstruction, the particles not accounted for by the tag are studied for consistency with the signal channel. Signal selection cuts are optimized for each of the different τ decay channels using simulated data.

Several kinds of backgrounds are present in this analysis. Combinatoric background events occur when particles are randomly reconstructed in a manner that happens to pass all of our signal selection cuts. The largest background consists of B^+B^- events in which the tag B meson has been correctly reconstructed and the remainder of the event contains particles from a real charged B that mimic the $B^+ \to \tau^+\nu_\tau$ decay.

The final set of cuts are imposed on the kinematic and angular properties of particles from the signal B. Since the neutrinos carry away significant amounts of energy, we expect the total energy of the reconstructed particles to be less than the energy input from the beams. The difference is known as "missing" energy and can also be expressed, via Equation 1, as missing mass, which is calculated from data: $M_{\mathrm{miss}} = \sqrt{(E_{\Upsilon(4S)} - E_{\mathrm{vis}})^2 - (\vec{p}_{\Upsilon(4S)} - \vec{p}_{\mathrm{vis}})^2}$. Here $(E_{\Upsilon(4S)}, \vec{p}_{\Upsilon(4S)})$ is the four-momentum of the $\Upsilon(4S)$, known from the beam energies. The quantities E_{vis} and $\vec{p}_{\mathrm{vis}}$ are the total visible energy and momentum of the event, which are calculated by adding the energy and momenta, respectively, of all the reconstructed charged tracks and photons in the event.

We further separate signal and background by exploiting the remaining energy (E_{extra}), calculated by summing the CM energy of the neutral clusters and charged tracks that are not associated with either the tag B or signal B. This is the most important variable is this analysis. Signal events tend to have low E_{extra} values whereas background events, which tend to contain additional sources of energy detected by *BABAR*, are distributed toward higher E_{extra} values. Therefore, the "signal region" is defined as a range of E_{extra}

beginning at zero. The other end is optimized for each individual τ decay channel as shown in Table 4. The E_{extra} "sideband" is defined as the range $E_{\text{extra}} > 0.5$ GeV. The signal selection efficiencies are defined as the fraction of true signal events reconstructed after a tag B has been reconstructed. These efficiencies are calculated using simulated data and summarized in Table 4.

4 Validation of Monte Carlo

Control samples are used to validate MC and define corrections to efficiencies of selection cuts. "Double-tagged" events, for which both of the B mesons are reconstructed in tagging modes ($B^- \to D^0 \ell^- \bar{\nu}_\ell X$ vs. $B^+ \to \bar{D}^0 \ell^+ \bar{\nu}_\ell X$), are used as the primary control sample. They are reconstructed from the same tag as our signal decay. Double-tagged events are similar to the signal events we hope to observe in many ways. Thus, the effects of our reconstruction and cuts on the double-tagged sample are useful for demonstrating that our MC is reliable and estimating our systematic errors.

As an example, the D^0 meson reconstructed mass distribution is shown in Figure 3 for the second tag in all double-tagged events. We see that the data and simulation agree well, which is one indication that the simulation is reliable. Agreement between data and MC is not always perfect; all of the disagreements we observe are a few percent or smaller. When a disagreement is observed, the MC is scaled to agree with data, and the error on that scaling is incorporated in our results as a systematic uncertainty.

"Single-tagged" events, in which one B decays via $B^- \to D^0 \ell^- \bar{\nu}_\ell X$ and the other B decay is not constrained, are also used. We determine the number of single-tagged events by subtracting the combinatoric component under the D^0 mass peak in events where one B is tagged but the second is allowed to decay without constraint. We determine this component by using D^0 mass sidebands, which are the flat regions away from the mass peak in Figure 4. We then average the yields from these combinatoric D^0 mass regions and scale by the ratio of the sideband and signal region widths. The resulting single-tagged event yields, and the double-tagged event yields, are shown in Table 5. We take the uncertainty on the data/MC single-to-double-tag ratios as the systematic uncertainty on the tag B yield. We find a correction of 1.05 with a 3.6% uncertainty.

We can further test the modeling of E_{extra} by comparing it in double-tagged events from data and MC. The E_{extra} for the double-tagged sample is calculated by summing the energy of the photons that are not associated with either of the tag B candidates. The sources of contributions to the E_{extra} distribution in double-tagged events are similar to those contributing to the E_{extra} distribution in the signal mode. We see good agreement between data and MC in Figure 5. The signal MC is included to illustrate how a signal from $B^+ \to \tau^+ \nu_\tau$ would look in a plot of E_{extra}; however, no actual $B^+ \to \tau^+ \nu_\tau$ events are present in the double-tagged sample.

5 Results

5.1 Background Prediction

After all cuts have been applied, a significant number of events from background sources will still be present in the signal region. The number of background events must be predicted in a reliable way; any excess above that prediction would be evidence of the signal $B^+ \to \tau^+ \nu_\tau$.

To ensure reliability, the background is predicted in two independent ways. First, in MC, we compute the ratio of events in the E_{extra} sideband ($N_{\text{MC,sb}}$) and signal ($N_{\text{MC,sig}}$) regions. Multiplying this ratio by the number of data events in the sideband ($N_{\text{data,sb}}$) yields a prediction of the number of background events in

the signal region in data ($N_{\text{exp,sig}}$):

$$N_{\text{exp,sig}} = N_{\text{data,sb}} \cdot \frac{N_{\text{MC,sig}}}{N_{\text{MC,sb}}}, \tag{3}$$

which is taken as the number of expected background events.

Second, this background estimate is validated by performing a similar test using sidebands in the D^0 mass distribution. Candidates in the sidebands represent a pure combinatoric background. We average the yields from the upper and lower sidebands and scale using the ratio of the D^0 mass sideband and signal region. This yields a D^0 mass combinatoric background estimate in the signal region for both data ($N^{\text{data}}_{\text{comb.}}$) and MC ($N^{\text{MC}}_{\text{comb.}}$). In the MC, the component of the background that contains real D^0 mesons is then computed:

$$N^{\text{MC}}_{\text{peak}} = N^{\text{MC}}_{\text{total}} - N^{\text{MC}}_{\text{comb.}}. \tag{4}$$

This is added to the combinatoric component, determined from data, to obtain an effective estimate of the total background,

$$N^{\text{predicted}}_{\text{total}} = N^{\text{MC}}_{\text{peak}} + N^{\text{data}}_{\text{comb.}}. \tag{5}$$

If our background estimates are reliable and robust, the results from two independent methods, $N^{\text{predicted}}_{\text{total}}$ and $N_{\text{exp,sig}}$, should agree. We find very good agreement, within uncertainties, between the two methods, as shown in Table 6.

5.2 Observed Data

In order to prevent bias on the part of the analysts, this analysis follows the standard procedure in *BABAR* of not examining (or "blinding") the data in the signal region until all cuts and background predictions are finalized. The final result is thus not known until the data are examined ("unblinded").

After finalizing the signal selection cuts, we unblind the data and measure the yield of events in each channel in the signal region, as shown in Table 7, together with the expected number of background events in the signal region (taken from the E_{extra} sideband prediction from Table 6). Figure 6 shows the E_{extra} distribution for all data and MC in the signal region, with signal MC shown for comparison.

We determine $\mathcal{B}(B^+ \to \tau^+\nu_\tau)$ from the number of signal candidates s_i in data for each τ decay channel, according to $s_i = N_{B^+}\mathcal{B}(B^+ \to \tau^+\nu_\tau)\varepsilon_{\text{tag}}\varepsilon_i$. N_{B^+} is the total number of charged B mesons in data; ε_{tag} and ε_i are the tag and signal efficiencies, respectively.

5.3 Calculation of $\mathcal{B}(B^+ \to \tau^+\nu_\tau)$ and Other Quantities

We use a modified frequentist method, known as the CL_s method (Read 2002), for calculating the branching fraction and upper limit. For this method, we generated a large number of simulated data distributions with different branching fractions in the range from zero to 10×10^{-4}. We define the "estimator" Q, which is monotonically increasing for increasing signal, and the confidence levels (CL) as follows:

$$Q \equiv \frac{\mathcal{L}_{s+b}}{\mathcal{L}_b}, \quad CL_{s+b} \equiv P_{s+b}(Q \le Q_{obs}), \quad CL_b \equiv P_b(Q \le Q_{obs}), \quad CL_s \equiv \frac{CL_{s+b}}{CL_b}. \tag{6}$$

$\mathcal{L}$ is the likelihood that a given number of observed events could be produced only by background (denoted with the subscript b) or by signal and background (denoted with the subscript $s+b$). $P_i(Q \le Q_{obs})$ is the fraction of simulated distributions that produced a Q less than or equal to the Q measured in data using a branching fraction that is positive ($i = s+b$) or zero ($i = b$). The branching fraction that maximizes $\log(Q)$ is taken as the most likely branching fraction. More technical details from both the central value and limit calculation are shown in Figure 7.

We set an upper limit at the 90% CL of

$$\mathcal{B}(B^+ \to \tau^+\nu_\tau) < 1.8 \times 10^{-4}, \tag{7}$$

and we determine the branching fraction to be

$$\mathcal{B}(B^+ \to \tau^+\nu_\tau) = (0.9 \pm 0.7(\text{stat.}) \pm 0.1(\text{syst.})) \times 10^{-4}. \tag{8}$$

Using the central value for $\mathcal{B}(B^+ \to \tau^+\nu_\tau)$ and taking the known values of G_F, m_B, m_τ, and τ_B (Particle Data Group 2006) and $|V_{ub}|$ from (Heavy Flavor Averaging Group 2006), we extract $f_B = 0.16^{+0.05}_{-0.08}$ GeV. Our branching fraction central value (Equation 8) is only significant at the level of 1.3σ. We find no evidence of physics beyond the SM. The Belle Collaboration, which operates a similar experiment in Japan, has reported evidence from a search for this channel where the branching fraction was measured to be $\mathcal{B}(B^+ \to \tau^+\nu_\tau) = (1.79^{+0.56}_{-0.49}(\text{stat.})^{+0.46}_{-0.51}(\text{syst.})) \times 10^{-4}$ (Belle Collaboration 2006).

6 Future Plans

This analysis will soon be submitted for publication to the journal *Physical Review D*. For my Ph.D. dissertation, I am refining this analysis further and attempting to measure $\mathcal{B}(B^+ \to e^+\nu_e)$ and $\mathcal{B}(B^+ \to \mu^+\nu_\mu)$, which have not yet been measured using the tag described in this paper.

References

Belle Collaboration. 2006. Evidence of the purely leptonic decay $b^- \to \tau^-\bar{\nu}_\tau$. *Physical Review Letters* 97.251802.

Cabbibo, Nicola. 1963. Unitary symmetry and leptonic decays. *Physical Review Letters* 10.531–532.

BABAR Collaboration. 2002. The babar detector. *Nuclear Instruments and Methods in Physics Research* A479.1–116.

GEANT4 Collaboration. 2003. Geant4: A simulation toolkit. *Nuclear Instruments and Methods in Physics Research* A506.250–303.

Halliday, David, Robert Resnick, and Jearl Walker. 1997. *Fundamentals of Physics*. New York, NY: John Wiley and Sons, Inc., fifth edition.

Heavy Flavor Averaging Group. 2006. Averages of b-hadron properties at the end of 2005. http://arxiv.org/pdf/hep-ex/0603003.

HPQCD Collaboration. 2005. The b meson decay constant from unquenched lattice qcd. *Physical Review Letters* 95.212001.

Kobayashi, Makoto, and Toshihide Maskawa. 1973. Cp violation in the renormalizable theory of weak interaction. *Progress of Theoretical Physics* 49.652–657.

Particle Data Group. 2006. Review of particle physics. *Journal of Physics* G33.1–1232.

Read, Alexander. 2002. Presentation of search results: The cl(s) technique. *Journal of Physics* G28.2693–2704.

A Tables

The data for Tables 1, 2, and 3 are taken from (Particle Data Group 2006).

Table 1: A summary of the fundamental constituents of matter is shown. The names of the particles and the symbols used to represent them are given. Also listed are their electric charge relative to the electric charge of the proton. For leptons, their mass, in units of MeV/c^2, is given. Notice all 12 particles are grouped into three generations of increasing mass and decreasing lifetime.

Leptons			Quarks		
Particle	Symbol	Charge	Particle	Symbol	Charge
electron	e^-	-1	up quark	u	$+\frac{2}{3}$
e neutrino	ν_e	0	down quark	d	$-\frac{1}{3}$
muon	μ^-	-1	charm quark	c	$+\frac{2}{3}$
μ neutrino	ν_μ	0	strange quark	s	$-\frac{1}{3}$
tau lepton	τ^-	-1	top quark	t	$+\frac{2}{3}$
τ neutrino	ν_τ	0	bottom quark	b	$-\frac{1}{3}$

Table 2: Properties of the composite particles relevant to this paper are shown. The same units are used in this table as in Table 1. The n is the neutron and $\bar{n}$ is the anti-neutron. A superscript "$+$" indicates that the particle has a positive electric charge. All particles with a symbol accompanied by no superscript (or a superscript "0") are electrically neutral. The quark content of the particles is given in parentheses next to the particle symbol.

Particle	Mass (MeV/c^2)	Lifetime (sec.)
n (udd)	939.56536 ± 0.00008	885.7 ± 0.8
$\bar{n}$ ($\bar{u}\bar{d}\bar{d}$)	939.56536 ± 0.00008	885.7 ± 0.8
$\Upsilon(4S)$ ($b\bar{b}$)	$(10.5794 \pm 0.0012) \times 10^3$	$\sim 10^{-23}$
B^+ ($\bar{b}u$)	5297.0 ± 0.6	$(1.638 \pm 0.011) \times 10^{-12}$
B^0 ($\bar{b}d$)	5279.4 ± 0.5	$(1.530 \pm 0.009) \times 10^{-12}$
D^0 ($c\bar{u}$)	1864.5 ± 0.4	$(410.1 \pm 1.5) \times 10^{-15}$
K^+ ($u\bar{s}$)	493.677 ± 0.016	$(1.2385 \pm 0.0024) \times 10^{-8}$
π^0 ($u\bar{u}/d\bar{d}$)	134.9766 ± 0.0006	$(8.4 \pm 0.6) \times 10^{-17}$
π^+ ($u\bar{d}$)	139.57018 ± 0.00035	$(2.6033 \pm 0.0005) \times 10^{-8}$

Table 3: Shown are the branching fractions of the τ decay modes used for $B^+ \to \tau^+\nu_\tau$ signal search .

Decay Mode	Branching Fraction
$\tau^+ \to e^+\nu_e\overline{\nu}_\tau$	(17.84 $\pm$ 0.06) %
$\tau^+ \to \mu^+\nu_\mu\overline{\nu}_\tau$	(17.36 $\pm$ 0.06)%
$\tau^+ \to \pi^+\overline{\nu}_\tau$	(11.06 $\pm$ 0.11)%
$\tau^+ \to \pi^+\pi^0\overline{\nu}_\tau$	(25.42 $\pm$ 0.14)%

Table 4: These are the selection cuts optimized for each signal τ decay mode. Additional selection cuts are described in the text. The signal efficiencies, multiplied by branching fraction, are given for each tau decay mode, relative to the number of tags. Values given in the squared parentheses represent lower and upper selection cuts imposed on the respective quantity. $R_{\rm cont.}$ is a variable developed to reject the background events using the angular qualities and masses of the particles in the event.

signal candidate	e^+	μ^+	π^+	$\pi^+\pi^0$
$M_{\rm miss}(\mathrm{GeV/c^2})$	[4.6, 6.7]	[3.2, 6.1]	≥ 1.6	≤ 4.6
$p^*_{\rm signal}(\mathrm{GeV/c})$	≤ 1.5	–	≥ 1.6	≥ 1.7
$R_{\rm cont.}$	[2.78, 4.0]	> 2.74	> 2.84	> 2.94
$E_{\rm extra}(\mathrm{GeV})$	< 0.31	< 0.26	< 0.48	< 0.25
Efficiency (%)	4.2 ± 0.1	2.4 ± 0.1	4.9 ± 0.1	1.2 ± 0.1

Table 5: Single-tag and double-tag yields in data and MC are shown for events where the D^0 meson from the first tag is required to decay as $D^0 \to K^-\pi^+$. We calculate the ratio of these two yields, and take the ratio of these ratios as a correction to the tagging efficiency determined from MC. The uncertainty on the correction is taken as a systematic error.

	Single Tags	Double Tags	Ratio ($\times 10^{-3}$)
Data	335417 ± 747	1067 ± 33	0.318 ± 0.098
MC	349972 ± 572	1065 ± 20	0.304 ± 0.057
Data/MC	-	-	1.049 ± 0.038

Table 6: This is the comparison of the expected total background, computed from data and MC in the D^0 mass sideband and signal regions, to that computed by projecting the $E_{\rm extra}$ sideband into the $E_{\rm extra}$ signal region.

	Background Prediction			
signal mode	e^+	μ^+	π^+	$\pi^+\pi^0$
$E_{\rm extra}$ sideband	44.3$\pm$5.2	39.8$\pm$4.4	120.3$\pm$10.2	17.3$\pm$3.3
D^0 sideband	44.2$\pm$6.4	42.8$\pm$6.0	113.4$\pm$11.6	16.3$\pm$4.5

Table 7: The observed number of on-resonance data events in the signal region are shown, together with number of expected background events. The background estimations include all applicable systematic corrections.

Signal τ Decay Mode	Expected Background Events	Observed Events in On-resonance Data
$e^+\nu_e\overline{\nu}_\tau$	41.9 ± 5.2	51
$\mu^+\nu_\mu\overline{\nu}_\tau$	35.4 ± 4.2	36
$\pi^+\overline{\nu}_\tau$	99.1 ± 9.1	109
$\pi^+\pi^0\overline{\nu}_\tau$	15.3 ± 3.5	17
All modes	191.7 ± 11.8	213

B Figures

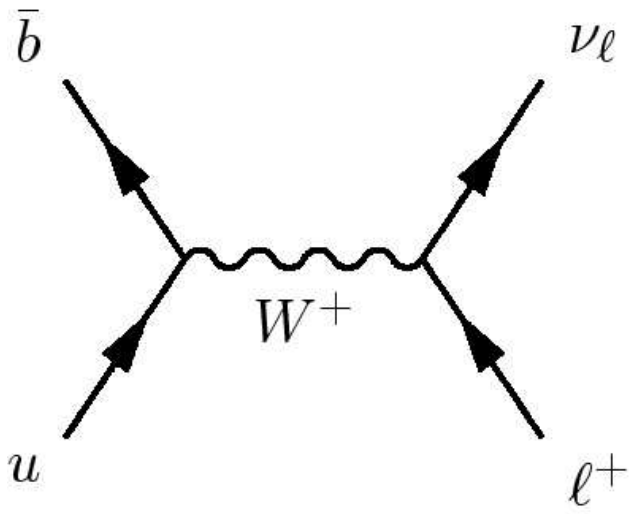

Figure 1: This is the diagram of $B^+ \to \ell^+ \nu_\ell$ decay via the weak interaction. The W^+ is one of the particles that mediates the weak interaction.

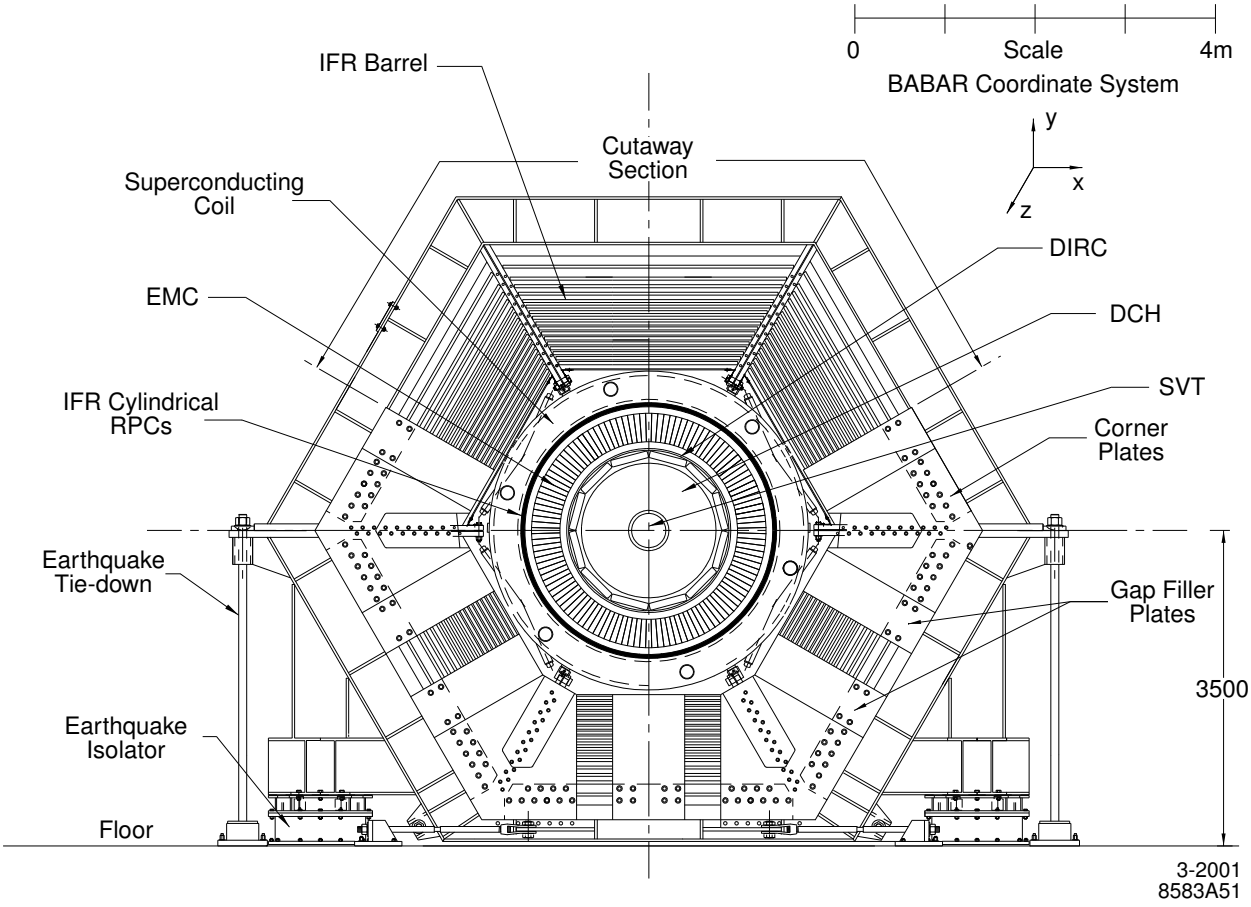

Figure 2: The *BABAR* detector is shown in cross-section. The Drift Chamber (DCH) detects charged particles via their ionization of gas withing the chamber. The Electromagnetic Calorimeter (EMC) is composed of scintillating crystals and detects energy deposited by neutral particles via light generated by the crystals. The superconducting coil generates a 1.5 T magnetic field to facilitate the measurement of charged particle momenta. Beams of e^+ and e^- travel along the z-axis and collide in the center of the detector within the Silicon Vertex Detector (SVT).

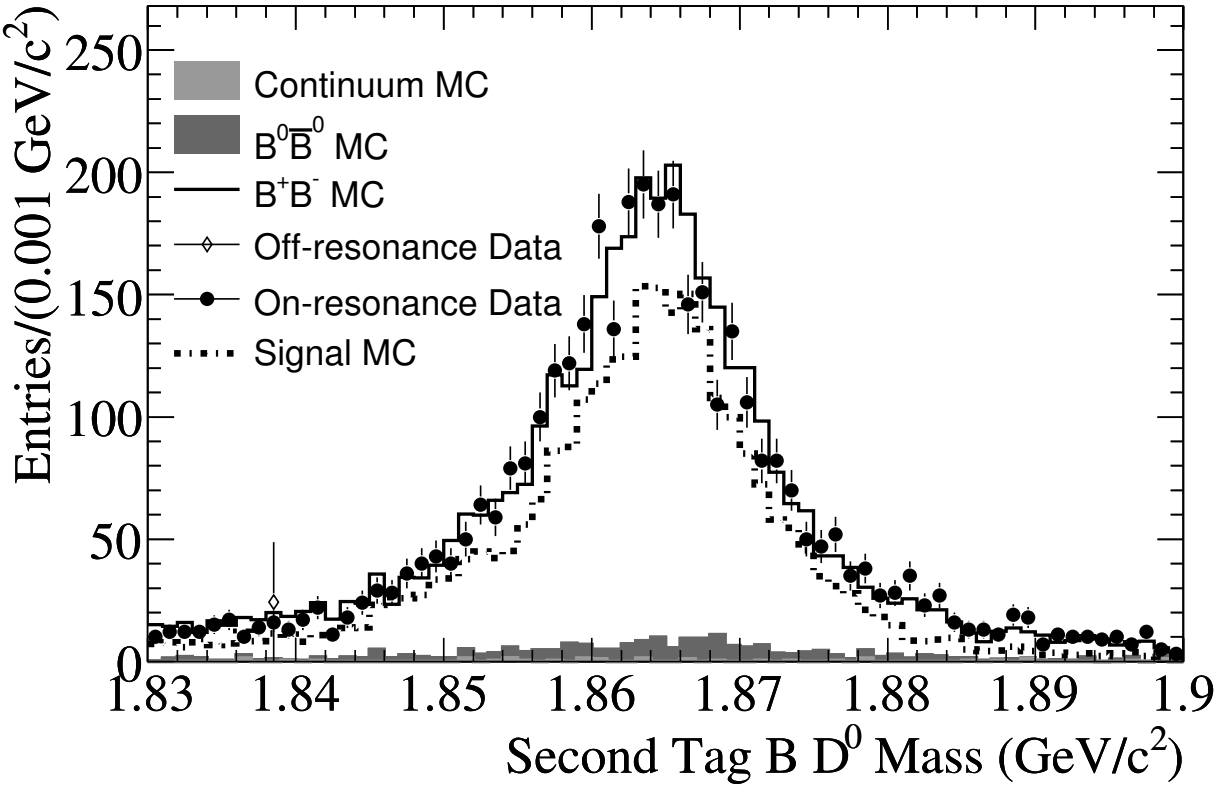

Figure 3: The D^0 reconstructed mass from the signal B meson in double-tagged events for on-resonance data (black circles) is shown along with the combined MC samples normalized to the data sample size. The $B^+ \to \tau^+\nu_\tau$ signal MC is shown for comparison, with arbitrary normalization.

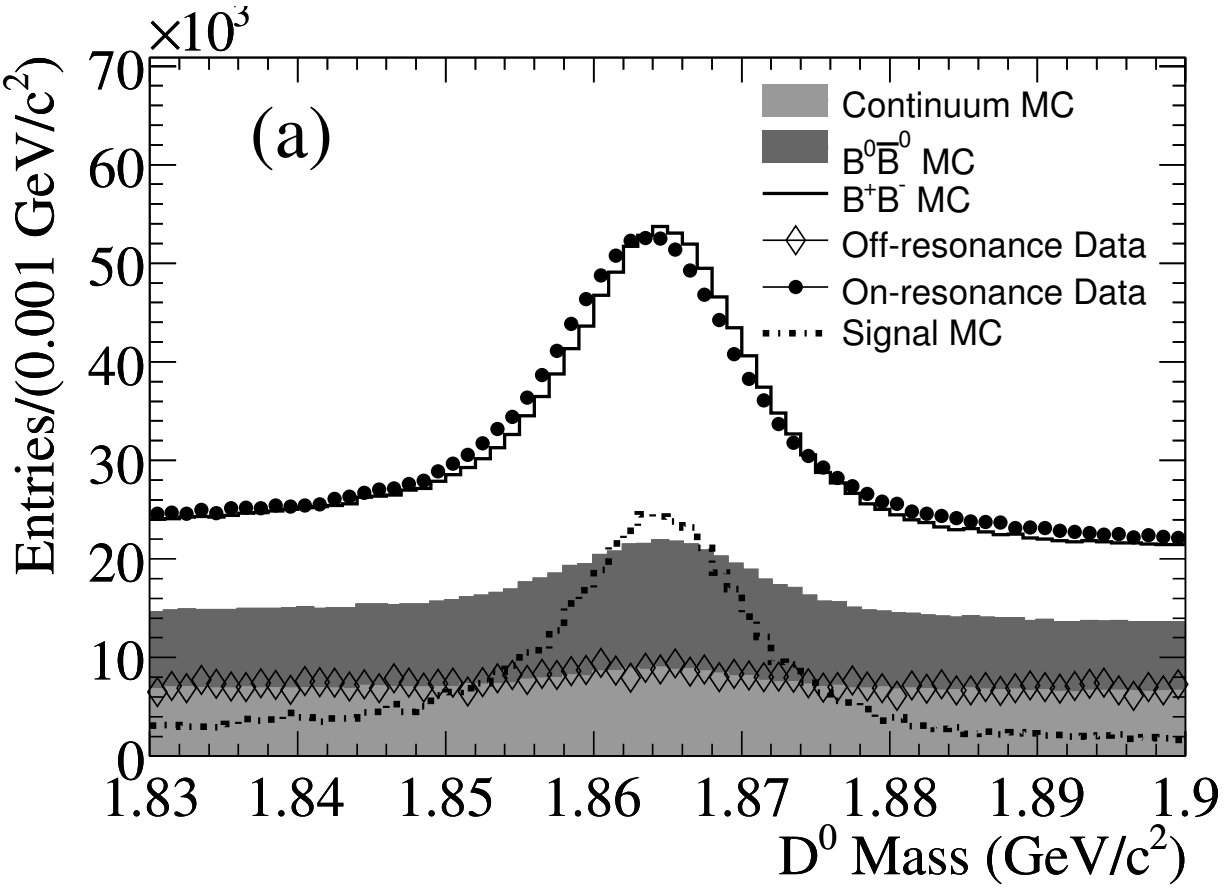

Figure 4: The reconstructed mass of the D^0 mesons from the tag B candidates with electrons in the tag is shown. The on-resonance data (filled circles) are overlayed on the $B\bar{B}$ MC and off-resonance background MC. Off-resonance data (open diamonds) are overlayed for comparison, as is the distribution from arbitrarily normalized signal MC (dashed-dotted line).

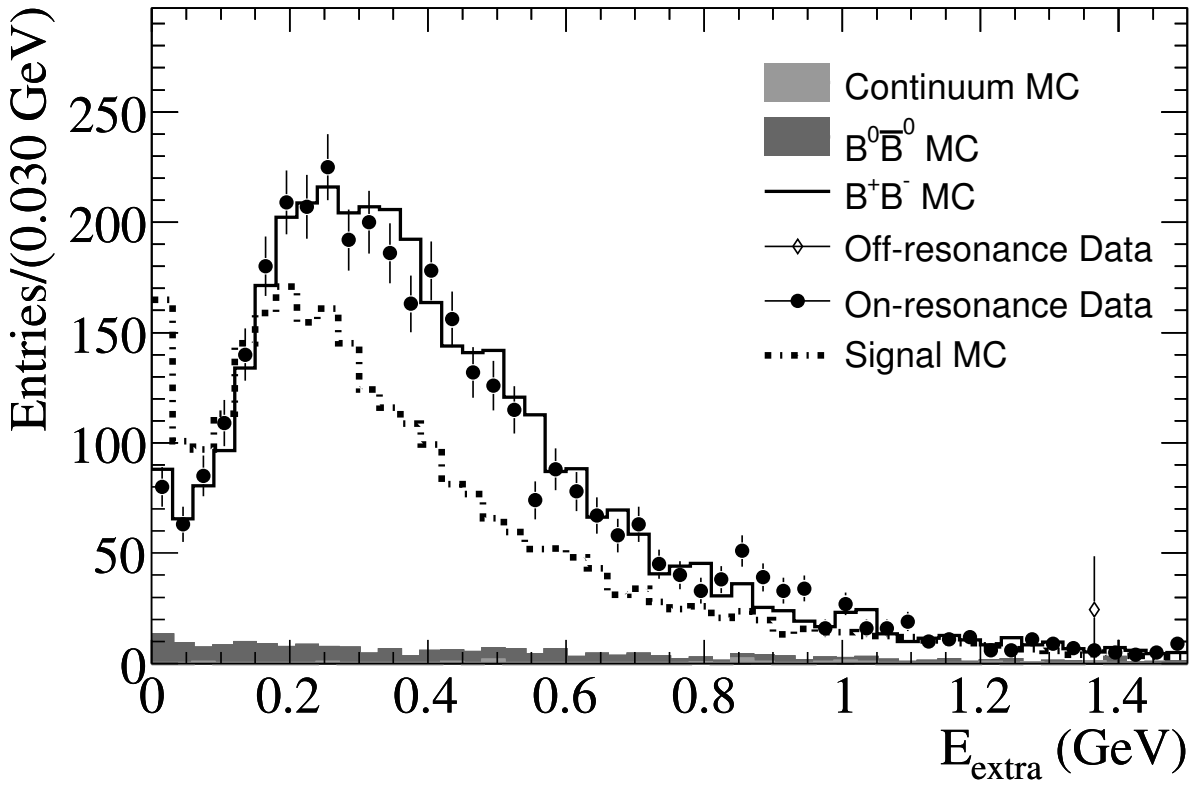

Figure 5: $E_{\rm extra}$ from the double-tagged samples is shown. On-resonance data (black circles) are overlayed on the combined MC distribution (histogram) with $B^+ \to \tau^+\nu_\tau$ signal MC (dashed-dotted line) shown for comparison, with arbitrary normalization.

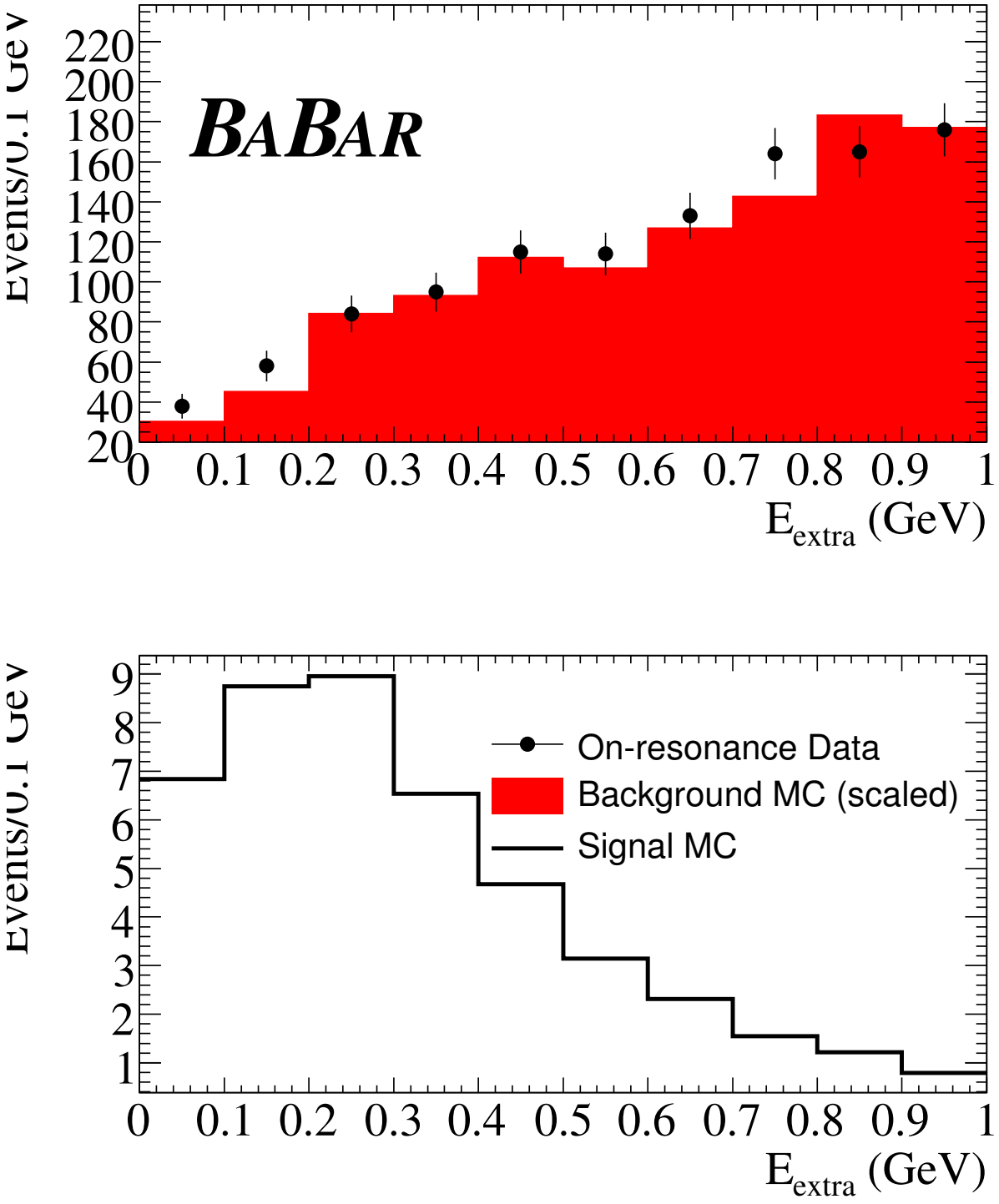

Figure 6: E_{extra} is shown after all cuts have been applied with all modes combined. MC have been normalized to the on-resonance data sample size. In addition, the background MC have been scaled to the data yield in the side band. Simulated $B^+ \to \tau^+\nu_\tau$ signal MC is plotted (lower) for comparison.

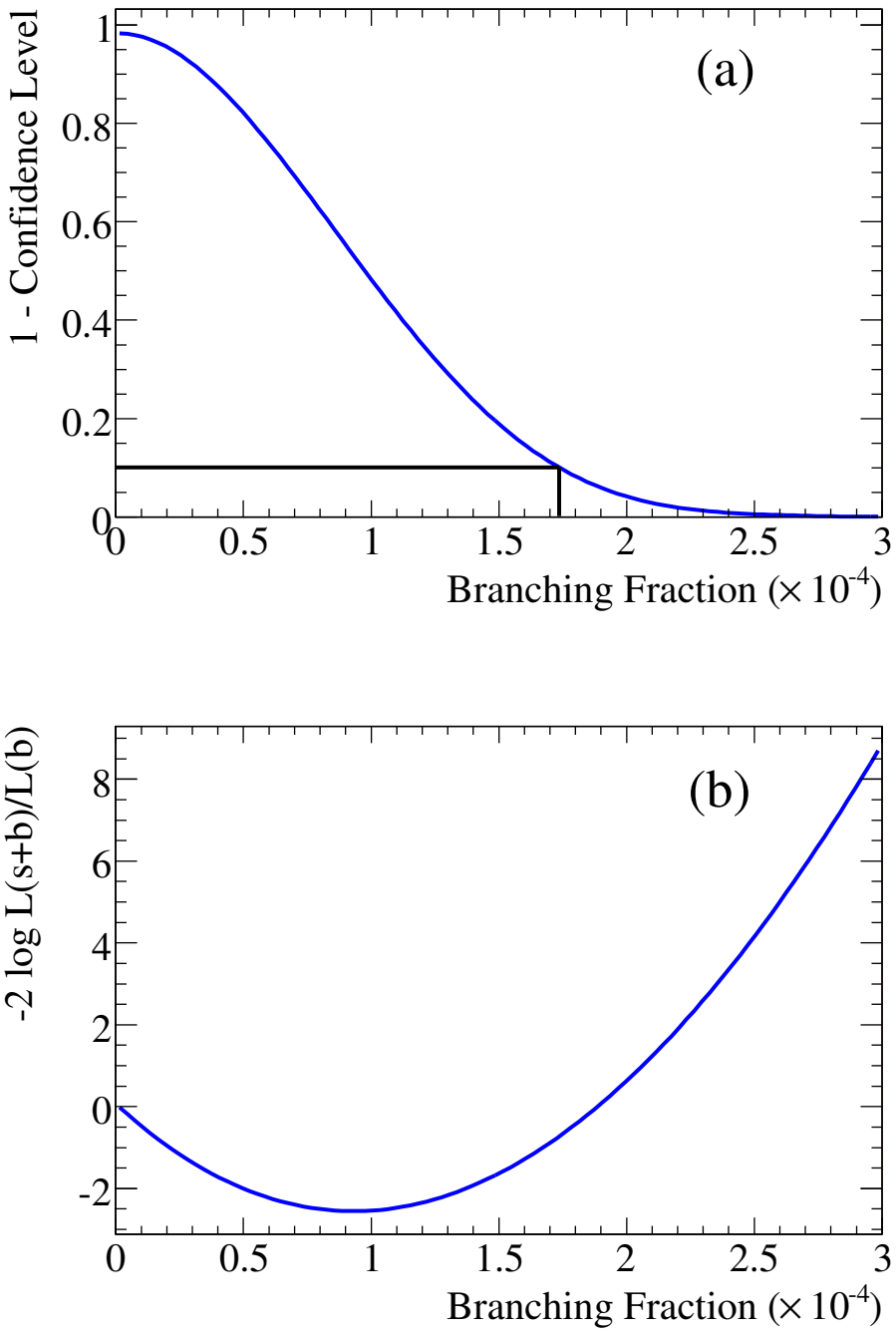

Figure 7: These are the curves determined from the likelihood ratio for (a) the upper limit calculation (where the horizontal and vertical intersecting lines indicate the 90% CL limit) and (b) the scan of the negative log likelihood ratio across signal branching fraction hypotheses, where the minimum indicates the most likely branching fraction central value and the points at one unit above the minimum correspond to the one standard deviation statistical uncertainties.